

Elsevier Editorial System(tm) for Dynamics of Atmospheres and Oceans
Manuscript Draft

Manuscript Number:

Title: The Makassar Strait Thermocline Variability at 20-40 Days

Article Type: Full Length Article

Keywords: 20-40 day variability; Makassar Strait; across-strait flow; isotherm displacements; eddies; eddy-resolving model

Corresponding Author: Mr. Kandaga Pujiana,

Corresponding Author's Institution: Lamont-Doherty Earth Observatory

First Author: Kandaga Pujiana

Order of Authors: Kandaga Pujiana; Arnold L. Gordon; E. Joseph Metzger; Amy Ffield

Abstract: The characteristics and plausible genesis of the 20-40 day variability observed within the Labani Channel, a constriction within the Makassar Strait, are described. The 20-40 day variability in Makassar Strait is trapped beneath the depth of the strongest stratification and evident in the across-strait flow, the across-strait gradient of the along-strait flow and in the vertical displacements of isotherms. The 20-40 day energy distribution of the across-strait flow is identifiable as a blue spectrum, demonstrating downward phase propagation. The flow fields are approximated by a vortex velocity structure, and the corresponding isotherm displacements imply potential vorticity conservation. We propose that the 20-40 day features observed in the Labani Channel are likely expressions of southward advected cyclonic and anti-cyclonic eddies. Analysis of simulated eddy kinetic energy from an eddy-resolving model further indicates that the upstream instability of the background flow within Makassar Strait is the energy source for the eddies which are then dissipated within the Labani Channel.

Highlights

>We examine the characteristics and plausible genesis of the 20-40 day variability in Makassar Strait. >The 20-40 day variability is evident in the across-strait flow, relative vorticity and in the vertical displacements of isotherms. > The 20-40 day variability is trapped beneath the depth of the strongest stratification. >We propose that the 20-40 day features are expressions of advected cyclonic and anti-cyclonic eddies. >An eddy-resolving model indicates that the upstream instability of the background flow within Makassar Strait is the energy source for the eddies.

The Makassar Strait Thermocline Variability at 20-40 Days

Kandaga Pujiana¹ and Arnold L. Gordon
Lamont-Doherty Earth Observatory, Palisades, New York

E. Joseph Metzger
Naval Research Laboratory, Stennis Space Center, Mississippi

Amy L. Field
Earth & Space Research, Upper Grandview, New York

¹ Corresponding author address: Kandaga Pujiana, Lamont-Doherty Earth Observatory, 61 Route 9W, Palisades, NY 10964.
E-mail: kandaga@ldeo.columbia.edu
Phone/Fax:(845) 365-8608/(845) 365-8175

1 Abstract

2 The characteristics and plausible genesis of the 20-40 day variability observed within the
3 Labani Channel, a constriction within the Makassar Strait, are described. The 20-40 day
4 variability in Makassar Strait is trapped beneath the depth of the strongest stratification
5 and evident in the across-strait flow, the across-strait gradient of the along-strait flow and
6 in the vertical displacements of isotherms. The 20-40 day energy distribution of the
7 across-strait flow is identifiable as a blue spectrum, demonstrating downward phase
8 propagation. The flow fields are approximated by a vortex velocity structure, and the
9 corresponding isotherm displacements imply potential vorticity conservation. We propose
10 that the 20-40 day features observed in the Labani Channel are likely expressions of
11 southward advected cyclonic and anti-cyclonic eddies. Analysis of simulated eddy kinetic
12 energy from an eddy-resolving model further indicates that the upstream instability of the
13 background flow within Makassar Strait is the energy source for the eddies which are
14 then dissipated within the Labani Channel.

15

16 Keywords: 20-40 day variability, Makassar Strait, across-strait flow, isotherm
17 displacements, eddies, eddy-resolving model

18

19

20

21

22

23

24 1. Introduction

25 Makassar Strait is the primary Pacific water inflow gateway to the Indonesian
26 Throughflow [ITF] (Fig. 1; Gordon and Fine, 1996). Observations made during 2004-
27 2006 indicated that the Makassar Strait throughflow contributed $12 \times 10^6 \text{ m}^3/\text{s}$ to the ITF
28 total of $15 \times 10^6 \text{ m}^3/\text{s}$ (Gordon et al., 2008; Gordon et al., 2010). The Makassar Strait
29 throughflow is not steady but rich of interannual and seasonal variability (Gordon et al.,
30 2010) as well as energetic fluctuations at tidal and intraseasonal [<90 day period]
31 timescales (Qiu et al., 1999; Susanto et al., 2000; Pujiana et al., 2009).

32 An earlier investigation of intraseasonal flow in Makassar Strait, using a 1.5 year
33 (1996-1998) time series of along-channel speeds at 300 m and 450 m, showed two
34 significant intraseasonal variability [ISV] peaks: 35-60 and 70-100 days (Susanto et al.,
35 2000). Estimates based on numerical experiments suggested that the two peaks were
36 directly linked to remote forcing emanating in the Western Pacific and Indian Ocean, as
37 well as baroclinic eddies originating in the Sulawesi Sea (Qiu et al., 1999; Masumoto et
38 al., 2001). The *International Nusantara Stratification and Transport* [INSTANT]
39 program from 2004 to 2006 (Sprintall et al., 2004; Gordon and Kamenkovich, 2010)
40 provides longer time series with improved vertical resolution of the Makassar Strait
41 throughflow. The Makassar along-strait flow observed by the INSTANT program reveal
42 that the 45-90 days variability characterizes the intraseasonal motions in the Makassar
43 Strait thermocline, and the vertical structure of the motions resembles that of remotely
44 forced baroclinic waves (Pujiana et al., 2009).

45 In this study we investigate the 20-40 day signatures within the Makassar Strait
46 thermocline and focus the analysis on the across-strait flow (a parameter that has been

47 overlooked in previous studies) data, relative vorticity derived from the along-strait flow
48 data at the two INSTANT moorings located across Makassar Strait and the temperature
49 fluctuations. Although the across-strait mean flow in Makassar Strait is smaller than the
50 along-strait mean flow (the maximum across-strait mean flow at the Labani Channel ~
51 $O(0.25 \text{ cm/s})$), its variance exhibits some interesting aspects. For example, the flow fields
52 at periods of 20-40 days show that the variances in the across-strait component are
53 comparable or larger than that in the along-strait direction at depths ranging from 100 to
54 300 m in the Makassar Strait thermocline. We propose that the pronounced 20-40 day
55 variability in the Makassar Strait thermocline derives its momentum from cyclonic and
56 anti-cyclonic eddies, which are advected southward with the mean Makassar Strait
57 throughflow. A better understanding on the 20-40 day features provides a fuller picture of
58 Makassar Strait intraseasonal flow.

59 The presentation of this paper is organized as follows. We will first describe the
60 data employed in section 2. Section 3 covers general descriptions of the 20-40 day
61 variability and their corresponding eddy characteristics from several parameters observed
62 in the Labani Channel. This is then followed by discussion on the eddy genesis in
63 Makassar Strait as simulated by an eddy-resolving model in section 4. The last section
64 concludes the paper with discussion and summary.

65

66 2. Data

67 The INSTANT program observed the ITF by means of moorings with ADCPs,
68 current meters, and temperature sensors, deployed at several Indonesian passages linking
69 the Pacific to the Indian Ocean (Sprintall et al., 2004). For this study we will be using the

70 INSTANT data within Makassar Strait. We also utilize several Conductivity,
71 Temperature, Depth [CTD] casts from the Arus Lintas Indonesia [ARLINDO] program
72 of 1993-1998 (Gordon and Susanto, 1999) and simulated velocity vectors from the
73 HYbrid Coordinate Ocean Model [HYCOM] (Metzger et al., 2010).

74

75 2.1. ADCP and Current Meter

76 The INSTANT 2004-2006 program monitored the ITF transport in Makassar Strait
77 from two moorings: $2^{\circ}51.9' \text{ S}$, $118^{\circ} 27.3 \text{ E}$ [MAK-West] and $2^{\circ}51.5' \text{ S}$, $118^{\circ} 37.7' \text{ E}$
78 [MAK-East], within the 45 km wide Labani Channel (Gordon et al., 2008; Fig. 1). Each
79 mooring consisted of an upward-looking RD Instruments Long Ranger 75 kHz Acoustic
80 Doppler Current Profiler [ADCP] at a depth of 300 m and four current meters deployed at
81 200, 400, 750, and 1500 m. The Mak-West and Mak-East moorings recorded ~3-year
82 long datasets from 2004 to late 2006. The datasets, horizontal velocity vectors, are
83 linearly interpolated onto a 25-m depth grid for each two-hour time step to produce
84 gridded current vectors from 50 to 450 m of water column. The gridded horizontal
85 current vectors are subsequently projected to the along (y) and across-strait (x) axis of the
86 Labani Channel, which are oriented along -10° and 80° (relative to north and positive is
87 clockwise) respectively (Fig.1), to yield gridded along (v) and across-strait (u) currents.

88

89 2.2. CTD

90 The CTD datasets used for this study are a compilation of several CTD casts
91 collected within or near Labani Channel during ARLINDO 1993-1998 cruises (Fig.1).
92 For each station, a Neil Brown Instrument System Mark III [NBIS MK III] CTD

93 measured conductivity, temperature and pressure within 12 hours period, yielding CTD
94 casts or temporal variability of measured parameters. CTD was lowered at a rate of 1 m s⁻¹,
95 and a 16 s⁻¹ sampling rate was selected. A phase lagging filter is applied to the
96 conductivity data as correction for the time constant mismatch. The data are then coarsely
97 de-spiked and reduced to a 1-dbar pressure series by applying a 5-scan median filter
98 around the target pressures.

99 A density profile inferred from several CTD casts within the Labani Channel shows
100 that the thermocline layer occupies a small fraction of water column from 25-450 m, with
101 the strongest stratification at mid-thermocline near 125 m separating the thermocline
102 from the lower thermocline (Fig. 2). Therefore the upper thermocline layer occupies a
103 thin layer from 25 to 100 m, while the lower thermocline layer lies at depths from 150 m
104 to 450 m.

105

106 2.3. Temperature Sensors

107 Several temperature and pressure sensors attached to Mak-West and Mak-East
108 moorings measured the temporal variability of the temperature profile in Makassar Strait.
109 Mak-West mooring provided better temperature profile resolution with 17 sensors
110 attached at different levels from 100 m to 400 m; Mak-East mooring only had 5 sensors.
111 The sensors sampled temperature and pressure at 6-minute intervals over a period of
112 almost 3 years from January 2004 to November 2006. The temperature datasets are
113 linearly interpolated onto a 25-m depth grid for each two-hour time step to provide the
114 gridded temperature data from 150 to 350 m of water column. Since the vertical structure

115 of temperature variability is less resolved at Mak-East mooring, we will only analyze the
116 temperature profile datasets from Mak-West.

117 To investigate the vertical structure of thermal field, mooring sensor temperature
118 data available in the lower thermocline layer are converted to vertical displacement (η).
119 Neglecting horizontal advection, diffusion, and heat sources, η is calculated using a heat
120 equation, which is simply a ratio between the gridded temperature amplitudes and the
121 vertical gradient of the averaged temperature, $\eta(z,t) = T(z,t) / \partial T / \partial z$, where z and t
122 denote depth and time respectively. The averaged temperature is a mean of the entire ~3-
123 year datasets. To remove the static stability effect from η , we normalize η with the ratio
124 between stratification frequency structure (determined from the CTD data shown in
125 Figure 2) and its corresponding vertical average, $\eta_n(z,t) = \eta(z,t)(N/N_o)$, where
126 subscript n and o are for normalized and vertically averaged respectively.

127

128 2.4. Simulated Data

129 Simulated velocity vectors and temperature variability from a numerical ocean
130 model are also used in this study. HYCOM has a horizontal resolution of $1/12.5^\circ \cos(\text{lat})$
131 $\times 1/12.5^\circ$ and employs 32 hybrid vertical coordinate surfaces with potential density
132 referenced to 2000 m. It has been shown to realistically simulate the circulation pathways
133 of the Indonesian Seas, and specific model formulation details can be found in Metzger et
134 al (2010). We examine daily data for a 3-year period from 2004 to 2006 within the
135 Makassar Strait thermocline, where the data are gridded vertically with a uniform
136 resolution of 25 m from the surface to 450 m of water column.

137

138 3. Description of the intraseasonal velocity and thermal fields

139 In this section, general characteristics of the Labani Channel velocity and
140 temperature profile variability measured are described. The statistical methods used to
141 explore those characteristics are mainly spectral method, cross-correlation in frequency
142 domain, and complex principal component analysis. Samples of velocity vector,
143 temperature, and across-strait gradient of v for several depths are given in Figure 3.

144

145 3.1. Observation

146 3.1.1. Horizontal and Sheared Flows

147 Gordon et al. (2008) using INSTANT data from 2004 to 2006 reported the vertical
148 and horizontal profiles of the Makassar Strait mean flow for sub-tidal variability and
149 found that \bar{v} revealed a distinct maximum southward ($-y$) speed at 140 m with western
150 intensification. The average direction of the flow points slightly to the east of along-axis
151 direction. Superimposed on the mean flow are the fluctuations (u' and v') across a broad
152 spectrum from inertial to interannual time frame. Focusing on the intraseasonal
153 variability and investigating the vertical profile of the variance attributed to along-strait
154 and across-strait flow, $\overline{u'^2(z)}$ and $\overline{v'^2(z)}$, where z denotes depth and over bar delineates
155 integration over intraseasonal periods, we find that the profile exhibits: the maximum \bar{v}'
156 is found closer to the sea surface, not at mid thermocline, while \bar{u}' attains maximum
157 magnitude at mid thermocline (Fig. 4a). The ratio between $\overline{u'^2(z)}$ and $\overline{v'^2(z)}$ suggests
158 that the intraseasonal motions are anisotropic throughout the Mak-West thermocline
159 depths (Fig. 4b), and $\overline{u'(z)} > \overline{v'(z)}$ for $75 \leq z \leq 225$ m. If the ratio were derived for
160 motions with periods of 20-40 days only, the depths where $\overline{u'(z)} > \overline{v'(z)}$ would then

161 extend from 75 to 275 m (not shown). Meanwhile Mak-East mooring shows that
162 $\overline{u'(z)} > \overline{v'(z)}$ is restricted to a thinner water column from 100 to 150 m (Fig. 4b).

163 The structure of variances for both velocity components versus depths (Fig. 4)
164 likely reflects the existence of various elements controlling intraseasonal motions at the
165 Labani Channel. For example, a topographically trapped baroclinic Kelvin wave, a
166 forcing that theoretically requires small transverse flow, may explain stronger signatures
167 of $\overline{v'(z)}$ at depths beneath 225 m. An analysis of v' at intraseasonal periods over
168 thermocline depths in Makassar and Lombok Straits suggests that remotely forced
169 baroclinic waves propagate from Lombok to Makassar Strait in the lower thermocline
170 depths (Pujiana et al., 2009). On the other hand, robust signatures of u' at intraseasonal
171 timescales over depths of 75-225 m maybe driven by a topographic Rossby wave or an
172 advected eddy whose dominant signal is expected to be in the normal component or x -
173 direction at the Labani Channel.

174 A spectral analysis is applied to the datasets to examine which periods within
175 intraseasonal timescales dominate the flow field variances in the Makassar Strait
176 thermocline. The power spectrum is computed using the multi-taper method with
177 adaptive weighing. Two distinct spectral peaks, 20-40 days and 45-90 days, generally
178 characterize the intraseasonal flows in the Makassar Strait thermocline. The 45-90 day
179 variability is a dominant feature in v' for throughout the thermocline depths and extracts
180 most of its energy from remotely forced baroclinic waves (Pujiana et al., 2009).

181 As for the 20-40 day variability, v' shows strong signature at 100-150 m of the
182 Mak-West water column, where the flow is well defined by a spectral peak centered at
183 30-day (Fig. 5a). A distinct monthly spectral peak is absent beneath 150 m of the Mak-

184 West thermocline although the 20-40 day variability energy does not change substantially
185 with depth. Some discrepancies are found from the Mak-East thermocline, however, in
186 which the spectral peak centered at a shorter period of 25-day is more dominant and
187 occurs deeper in the lower thermocline from 225 to 300 m (Fig. 5b). Furthermore, relative
188 vorticity (ζ') computed from v' of both moorings, shows significant variance associated
189 with monthly variation. A broad spectral peak of 20-40 day centered at a period of 30-day
190 characterizes ζ' at depths that extend from the base of the upper thermocline to the lower
191 thermocline layer, and its energy is comparable or larger than that attributed to the 45-90
192 day variability (Fig. 5c).

193 The signature of the 20-40 day variability over the Makassar Strait thermocline is
194 more pronounced in the u' data. The vertical distribution of energy density of u' at
195 intraseasonal timescales for several depths (Fig. 6a,b) indicate that the spectrum shape
196 transforms from red to blue spectrum as depth increases from 100 to 175 m; a blue
197 spectrum with a distinct spectral peak centered at 25-day gains energy with depth. Deeper
198 in the lower thermocline, the spectral peak of the 20-40 day variability tends to be
199 centered at a longer period of 30-day. The Mak-East mooring also shows a similar pattern
200 of the 20-40 day variability in the lower thermocline (Fig. 6b). The 20-40 day variation
201 observed from the Mak-East is also linked to that observed from the Mak-West as more
202 than 80% of variance attributed to the 20-40 day variability from both mooring is
203 statistically coherent. In addition to being coherent, the 20-40 day variability from the
204 two moorings does not exhibit a significantly different from zero phase shift, a fact which
205 may indicate that the 20-40 day variability has its horizontal scale across the strait larger
206 than the ~19 km distance separating the moorings.

207 Another unique feature from u' varying at periods of 20-40 days, which is
208 synonymously observed from both mooring, is a pattern of phase shift over depths:
209 $u'(z + dz)$ tends to flow slower than $u'(z)$ with a constant lag. On a time and depth plot of
210 u' at a 20-40 day period band (Fig. 7a), we draw lines, where each line connects the flow
211 that has the same phase, i.e. phase lines. And those lines are uniformly tilted downward at
212 an almost constant angle, indicative of a downward phase propagating feature. This
213 downward phase shift found from u' differs from the phase shift of dominant variability
214 in v' . Pujiana et al. (2009) suggested that the most dominant period band of v' observed in
215 the Makassar Strait thermocline exhibited upward phase propagation, which transferred
216 energy downward to deeper depths at a speed of 25 m/day. To further elucidate the 20-40
217 day variability from u' in Makassar Strait, we isolate the variability of interest from raw
218 data using a band pass filter with cut off periods of 20 and 40-day. A complex principal
219 component (CPC) analysis is then applied to the filtered data, which principally
220 decomposes the data into several modes constituting substantial percentage of variance
221 contained in the data, and solely focuses on the filtered across-channel flow data in the
222 lower thermocline. The CPC analysis indicates that up to 90% of u' within a period band
223 of 20-40 days can be explained by the first three eigenvectors, where the first mode
224 describes 50% variance and the next two modes denote 25% and 15% variance
225 respectively.

226 From the eigenvector profile, we learn how the amplitudes of u' vary with depth.
227 The first mode eigenvector reveals maxima at 175 m and at 250 m (Fig. 7b) where two
228 distinct spectral peaks of 25-day and 30-day are also observed: the energy associated with
229 the spectral peak centered at 25-day is maximum at depth of 175 m, while the energy

230 attributed to the 30-day variability is maximum at depth of 250 m. Therefore the vertical
231 energy distribution for the 20-40 day across-channel flow is well resolved by the first
232 eigenvector. Moreover, the relative phase inferred from the ratio between the imaginary
233 and the real part of the first eigenvector signifies a phase increase with a rate of $1.7^\circ/\text{m}$
234 towards greater depths (Fig. 7b). The rate of phase shift implies that it would take around
235 20 days for the 25-day oscillation to propagate from 125 m to 300 m of water column.
236 This relative phase structure is better understood from reconstructed data obtained
237 through a multiplication between eigenvectors and their corresponding principal
238 components (time series). A plot of reconstructed u' based on eigenvector and principal
239 component for the first mode captures the phase shift nature revealed by the eigenvector
240 profile: periodic 20-40 day variability with phase lines tilted downward at a uniform
241 angle (Fig. 7c). Thus the unique downward phase propagation feature contained in the
242 filtered 20-40 day u' data can be resolved and replicated by only the first mode.

243

244 3.1.2. Vertical displacement

245 The vertical displacement of the isotherms within Makassar Strait is rich in
246 intraseasonal features (Fig. 3b). Figure 3b demonstrates that significant variance
247 associated with 25-day oscillation also characterizes temperature fluctuations at 150 m
248 and greater depths. The vertical scale of the temperature variability within a period band
249 of 20-40 days is likely larger than the lower thermocline thickness, as the correlation
250 between temperature variability at different depths shows that 70% temperature variance
251 at 150 m is coherent with that at 300 m (not shown). Thermal field at intraseasonal
252 timescales within Makassar Strait shares a similar power spectrum pattern (Fig. 6c) with

253 the across-strait flow data as the variability shows significant 20-40 day variation, and it
254 is likely that the two parameters are physically linked.

255

256 3.1.3. Cross-correlation analysis

257 The following analysis discusses relationship between two different parameters,
258 with the objective of establishing a reasonable link between the dominant variability,
259 particularly that at 20-40 days, discussed previously. The correlation method used here is
260 a cross-spectral analysis, which identifies variations of high energy in the same spectral
261 frequency bands. The method also computes phase difference between the parameters,
262 which is useful for further explaining the two strongly linked parameters that may share a
263 common dynamical process. We investigate the correlation between velocity vectors and
264 isothermal displacements.

265

266 3.1.3.1. Across-strait flows versus vertical displacements of isotherms

267 We have shown that u' and η' observed in the Makassar Strait thermocline share a
268 common spectral shape, of high energy for the period band of 20-40 days (Fig. 6),
269 whereas about 80% variance of u' can explain that of η' . The degree of coherence
270 between the two variables observed at depths of 150-225 m is significantly above the
271 95% confidence level for a range of periods from 20-30 days (Fig. 8a).

272 In terms of phase difference, the coherence analysis shows that u' and η' that fall
273 within a period band of 20-40 days are approximately in phase, which may explain that
274 the isotherms adiabatically shoals, as the eastward across-strait flow gains momentum.
275 On the other hand, when the eastward flow starts decelerating and turning westward,

276 isotherms are pushed down to shift the thermocline to greater depth. The relation between
277 isotherm displacement and across-strait flow can be expressed as $\overline{u'\eta'} > 0$.

278 Does the relation give rise to zonal heat flux? To examine whether the relationship
279 between η' and u' does refer to heat transport, the horizontal gradient of temperature
280 across the strait needs to be determined, which unfortunately can not be resolved using
281 the observed data due to unavailability of temperature data at Mak-East. It thus can be
282 summarized that for the variability at 20-40 day timescale within the lower thermocline
283 of the Makassar Strait, the eastward across-strait flow corresponds to shoaled
284 thermocline, while the westward across-strait flow relates to deepening thermocline.

285

286 3.1.3.2. Along-strait flow versus across-strait flow

287 Distinct spectral peaks covering periods of 20-40 days centered at 30-day are
288 observed at depths of 100-150 m from Mak-West, but their signatures are somewhat
289 obscured by the red spectrum profiles of the along-strait flow variability. At Mak-East,
290 25-day oscillation dominates the 20-40 day variability and is evident at depths greater
291 than 200 m. Meanwhile across-strait flow consistently displays 20-40 day variations over
292 the lower thermocline layer from both moorings. We now examine whether the 20-40 day
293 variability in the across-strait flow data is a projection of turbulent fluctuations on the
294 mean flow that transports momentum across the strait.

295 The instantaneous rate of along-strait momentum transfer in the across-strait
296 direction is defined as $\rho_o(V + v')u'$, where V is the mean flow, and u' and v' are velocity
297 fluctuations in the across-strait and along-strait directions respectively. The average rate
298 of flow of along-strait momentum in the across-strait direction is therefore

299 $\rho_o \overline{(V+v')u'} = \rho_o V \overline{u'} + \rho_o \overline{v'u'} = \rho_o \overline{v'u'}$, as $\overline{u'} = 0$. The Reynolds stress, $\rho_o \overline{v'u'}$, is
 300 approximated with a cross-correlation between v' and u' . Structure of $\overline{v'u'}$, normalized
 301 by their variances, averaged over intraseasonal periods shows that $\overline{v'u'} < 0$ (Fig. 9a),
 302 which implies a westward (eastward) eddy flux of southward (northward) momentum.
 303 The correlation coefficient in frequency domain (Fig. 9b) indicates that the 20-40 day
 304 variability contributes substantially, particularly that in the lower thermocline.

305 Another way to interpret $\overline{v'u'} < 0$ is in terms of the turbulence. The vertical
 306 structure of the mean flow (the time average of subinertial flow) observed at the
 307 Makassar Strait moorings indicates that the flow is directed southward and found with a
 308 maximum within the Mak-West thermocline below 50 m (Fig. 10). More energetic Mak-
 309 West flow yields positive mean zonal shear and relative vorticity ($\overline{\partial v'/\partial x} > 0$). Assume
 310 that a particle at a point between Mak-West and Mak-East sites instantaneously moves
 311 eastward ($u' > 0$). The particle retains its original velocity during the migration, and when
 312 it arrives at Mak-East it finds itself in a region where a smaller velocity prevails. Thus the
 313 particle tends to speed up the neighboring fluid particles after it has reached the Mak-East
 314 site, and causes a more negative (southward) v' . Conversely, the particles that travel
 315 westward ($u' < 0$) tend to drag v' down. In this way turbulence tends to diffuse and
 316 attenuate the across gradient of the mean flow, $\overline{\partial v'/\partial x} > 0$.

317

318 3.1.3.3. Relative vorticity versus across-strait flow

319 The across-strait gradient of v' inferred from Mak-West and Mak-East data
 320 demonstrates that the 20-40 day variability constitutes significant variance of sheared v'
 321 in the Makassar Strait lower thermocline (Fig. 5c). We now demonstrate how relative

322 vorticity fluctuation (ζ') introduced by sheared v' that relates to u' , also reveals clear
 323 signature of the 20-40 day variability. Plots of ζ' overlaid on u' at the same depth for
 324 several levels display that both parameters do not show similar intraseasonal fluctuations
 325 within the upper thermocline layer but seem in concert for the lower thermocline (Fig.
 326 11a). It is shown in Figure 11a that positive ζ' corresponds with eastward flow, while
 327 negative ζ' relates to westward flow. The similarity in fluctuation between ζ' and u'
 328 over intraseasonal periods in the lower thermocline is primarily contributed by the 20-40
 329 day variability (Fig. 11b).

330

331 3.1.4. Eddy-like features from observation

332 In previous sections we have discussed general characteristics of the 20-40 day
 333 variability in the Makassar Strait thermocline extracted from datasets obtained at the
 334 Labani Channel of Makassar Strait. At least three interesting features attributed to the 20-
 335 40 day variability were obtained from the datasets.

336 1. The u' is more energetic than v' at depths extending from 100 m to 250 m.
 337 Although inferring the two-dimensional motion from two points is inherently tricky, we
 338 suspect that a dominant across-strait flow at the Labani Channel may relate to an eddy
 339 advected by the ITF. Assume an eddy propagates along a mean flow, $V(t) + iU(t)$, that is
 340 spatially uniform but varying with time, the eddy's path can be projected into a complex
 341 plane as $y'(t) + ix'(t) \equiv r(t)e^{i\phi(t)}$. The currents observed by a mooring are then given as
 342 (Lilly and Rhines, 2001)

$$343 \quad \xi(t) \equiv V + iU - ie^{i\phi} \tilde{v}(r) \quad (1)$$

344 where $\tilde{v}(r)$ is the radial velocity of the eddy and r is the distance from the mooring to the
345 eddy center. If the eddy dynamics is simplified as a Rankine vortex, $\tilde{v}(r)$ can be
346 expressed in the following formula

$$347 \quad \tilde{v}(r) = \begin{cases} VrR^{-1}, r < R \\ Vr^{-1}R, r > R \end{cases} \quad (2)$$

348 where V is the maximum azimuthal velocity, and R marks the eddy core radius that has
349 uniform potential vorticity. Since the ITF flows in the y -direction at the Labani Channel,
350 the observed eddy currents, by virtue of eq. (1) and (2), then are always perpendicular to
351 the along-strait axis or in the across-strait component. Therefore, the observed flow
352 associated with the eddy would be more dominant in u' than in v' .

353 2. The 20-40 day variability displays relationship between u' and ζ' : eastward
354 flow is linked to positive relative vorticity, while westward flow corresponds with
355 negative relative vorticity (Fig. 11). This strong link between u' and ζ' is well
356 approximated by eq. (2), which states that positive (negative) radial velocity or eastward
357 (westward) current is fulfilled when the maximum azimuthal velocity associated with a
358 vortex is positive (negative). And positive (negative) azimuthal velocity must
359 characterize an anti-cyclonic (cyclonic) eddy, which simultaneously coincides with
360 positive (negative) relative vorticity as schematically given in Figure 12. A positive
361 relative vorticity field corresponds with an anti-cyclonic eddy at the Labani Channel,
362 noting that the channel is located at the southern hemisphere.

363 3. The thermal field and relative vorticity are linked at the Labani Channel. The
364 isopycnals in the lower thermocline layer dip down when the flow field exhibits negative
365 relative vorticity (Fig. 13a). Meanwhile the isopycnals shoal as the relative vorticity

366 observed in the Labani Channel lower thermocline turns positive (Fig. 13b). We suspect
367 that the vertical displacements of isopycnals varying at periods of 20-40 day in the lower
368 thermocline of the Labani Channel are direct responses to water column squeezing or
369 stretching attributed to cyclonic or anti-cyclonic eddies. Given the Brunt-Väisällä
370 structure in the vicinity of the Labani Channel (Fig. 2), we assume a one and half-layer
371 model to govern the stratification in the Makassar Strait thermocline with the strongest
372 thermocline at depth of 125 m acting to demarcate the two layers. The upper thermocline
373 layer is set to be motionless for 20-40 day timescales as the activity of 20-40 day
374 variability is weak. Because across-strait gradient of v' is present in the lower
375 thermocline, ζ' is introduced into the lower thermocline as discussed in the previous
376 paragraph. To conserve potential vorticity, $q = (\zeta + f)/h_2$, where h_2 is lower thermocline
377 thickness, h_2 should squeeze (stretch) when the layer acquires negative (positive) relative
378 vorticity. Coriolis acceleration (f) is negligible as the mooring site is close to the
379 equator.

380 After reviewing the observations discussed in previous sections, we hypothesize
381 that the features attributed to the 20-40 day variability from the moorings at the Labani
382 Channel are linked to eddy dynamics, and the next step is to describe where the eddies
383 originate from. Several numerical experiments (Qiu et al., 1999; Masumoto et al., 2001)
384 indicated that eddy activities at intraseasonal timescales are intense within the Sulawesi
385 Sea, a basin located to the north of Makassar Strait (Fig. 1). Masumoto et al. (2001)
386 estimated that eddies with a period of 40-day were internally generated in Sulawesi Sea
387 and affected the ITF transport in Makassar Strait. However the Sulawesi eddies that the
388 study of Masumoto et al. (2001) numerically estimated were not only trapped in the lower

389 thermocline but rather occupied a thick water column extending from the surface to 1000
390 m isobath. To investigate the generating mechanism of eddies at the Labani Channel, we
391 analyze the output of an eddy resolving numerical models in Makassar Strait, and the
392 discussion is given in the following section.

393

394 4. The 20-40 day variability in an eddy-resolving model

395 As described earlier, flow and thermal field from two moorings at the Labani
396 Channel of Makassar Strait reveal clear 20-40 day variability features, which we propose
397 are related to cyclonic and anti-cyclonic eddies. To further examine the spatial variation
398 and origin of the 20-40 day variability, we investigate the model output of a global
399 HYCOM experiment (Metzger et al., 2010). We focus our analysis on the model flow at
400 intraseasonal timescales in the Makassar Strait and Sulawesi Sea thermocline.
401 Comparison between the model output and observation at the Mak-West and Mak-East
402 mooring sites indicates that the numerical experiment underestimates the Makassar Strait
403 throughflow due to inaccurate model topography, where the Dewakang Sill (Fig. 1),
404 located near the southern end of the strait, was introduced 195 m too shallow in the model
405 (Metzger et al., 2010). In addition to weaker simulated mean transport, the study of
406 Metzger et al. (2010) also showed that shallower sill depth assigned in the model caused
407 the maximum simulated southward flow in Makassar Strait to be ~50 m deeper than
408 observed.

409 The model u' at intraseasonal timescales qualitatively agrees with observation at
410 Mak-West and Mak-East moorings: the 20-40 day variability has clearly larger energy
411 than other intraseasonal periods, and the variability at Mak-West is more energetic than

412 that at Mak-East (Fig. 14a,b). It is also shown in Figure 14a,b that the distinct monthly
413 spectral peak is well simulated at depths greater than 200 m, which is 50-75 m deeper
414 than the depth where observation starts to record the monthly peak. The discrepancy is
415 again due to inaccurate sill depth. Monthly variation also occurs in the model ζ'
416 simulated at the mooring locations. Like the observation, the model ζ' and u' at depths
417 beneath 200 m are linked: positive relative vorticity correlates with eastward flow, while
418 negative vorticity corresponds with westward flow (not shown). A coherence analysis
419 between the model ζ' and u' for several depths within the thermocline layer of Mak-
420 West site displays that both parameters varying at intraseasonal timescales are strongly
421 coherent for a period band of 20-40 days, and the strongest correlation is found at depths
422 greater than 200 m (not shown). Thus the numerical experiment is able to capture some
423 general features of the 20-40 day variability, which are similarly revealed from
424 observation at the mooring sites in the Labani Channel.

425

426 4.1. Eddy signature and its genesis in Makassar Strait

427 The next questions we explore within the model output are what causes the 20-40
428 day variability? Where does the forcing originate from? And why is the strong 20-40 day
429 variability trapped within the lower thermocline. To determine the ocean dynamics
430 responsible for the pronounced 20-40 day fluctuations, the simulated flow field attributed
431 to the period band of interest in the Makassar Strait is analyzed. We first want to gain
432 insights on the space and time evolution of a motion that may drive the ζ' fluctuations in
433 Makassar Strait. For example, an event of negative ζ' is inferred from two moorings at
434 250 m in the Labani Channel on 17 December 2005 (selected to be representative of

435 positive ζ' events), and it is assumed that an anticlockwise eddy-like motion causes the
436 ζ' field. The model agrees well with observation to simulate positive ζ' at 250 m of the
437 Labani Channel thermocline on 17 December 2005, and the model flow field shows that
438 the positive ζ' value does correspond with with a counter clockwise vortex motion with a
439 diameter of ~ 40 km squeezed in the narrow Labani passage (Fig. 15). Assume quasi-
440 geostrophic dynamics govern the vortex observed and simulated in the Labani Channel,
441 the vortex diameter will be approximately as large as the local internal radius
442 deformation, which is function of N , coriolis acceleration (f), and water depth (H). The
443 deformation radius for the first oceanic mode in the Labani Channel falls within $O(\sim 275$
444 km), substantially larger than the channel width itself. Therefore the eddy size in
445 Makassar Strait is more likely topographically constrained. The model velocity and
446 relative vorticity fields at the Labani Channel for over a period of ~ 3 years (2004-2006)
447 display 23 events of anti-cyclonic vortex motion and 17 episodes of cyclonic eddy-like
448 features.

449 Furthermore, following the spatial and temporal eddy core variability, it can be
450 inferred that the eddy-like motion is not locally generated at the Labani Channel but
451 seems rather to propagate from the northern Makassar Strait into the Labani Channel. It is
452 shown in Figure 15 that an anti-cyclonic eddy with a diameter of ~ 100 km has its core
453 located at latitude of 2°S and is simulated on 7 December 2005, and the eddy diameter is
454 reduced as it propagates southward with a phase speed of 0.25 m/s before occupying the
455 Labani Channel on 17 December 2005. After reaching the Labani Channel, the eddy
456 dissipates and its signature is not simulated further south (not shown).

457 The model eddy occurs only within the lower thermocline and is identifiable as a
458 feature that has homogeneous ζ' over depths. A depth versus distance plot of ζ' along a
459 transect given in Figure 1 shows that a homogeneous positive ζ' over depths extending
460 from 200 to 350 m marks the event of an anti-cyclonic eddy on 17 December 2005 in the
461 Labani Channel (Fig. 16). Thus the eddy varying at periods of 20-40 days in Makassar
462 Strait is trapped within the lower thermocline. Several snapshots of simulated horizontal
463 flow fields and structure of ζ' in Makassar Strait (Fig.15, 16) provide spatial and
464 temporal dimension of the motions that likely force the 20-40 day variability observed at
465 the Labani Channel. It is shown that circular motions develop at 2°S or farther north and
466 propagate southward in Makassar Strait. To better map out the source region of the
467 vortices, we analyze simulated eddy kinetic energy (EKE) budget over an expanded
468 region including the Sulawesi Sea (Fig. 1), a basin with robust intraseasonal activities
469 (Qiu et al., 1999; Masumoto et al., 2001, Pujiana et al., 2009). Although detecting energy
470 radiation through EKE can be ambiguous, the intraseasonal variability can be
471 characterized by a suitably specified EKE.

472 The EKE budget is deduced from the rapidly-varying segment of u and v , with an
473 assumption that each variable has a slowly-varying part and a rapidly-varying part,
474 labeled as (u,v) and (u',v') respectively. The rapidly-varying part oscillates at periods of
475 20-40 days, and the EKE density is therefore defined as $0.5\rho_o(u'^2+v'^2)$, where ρ_o is the
476 background density, vertically averaged over depths from the potential density structure
477 given in Figure 2. Comparison of the averaged EKE (Fig. 17) at several depths clearly
478 exemplifies the basins with the most pronounced EKE in the region: Sulawesi Sea (A),
479 northern Makassar Strait (B), and Southern Makassar Strait (C), where the Labani

480 Channel demarcates the separation between the northern and southern of Makassar Strait.
481 Nevertheless we consider basins A and B as the only viable energy source areas for eddy
482 activities at the Labani Channel as we expect the eddy to be advected, along with the ITF,
483 southward into the channel. In area A, the eddy activity is significant close to the surface
484 and decays away from it, and the eddy likely does not extract its energy from the wind
485 because the atmospheric perturbations over the area lacks a 20-40 days variability (not
486 shown). The eddy might instead relate to instabilities of the Mindanao currents occurring
487 on the eastern Mindanao coasts or be a Sulawesi basin scale response to the periodic
488 Mindanao currents (Qiu et al., 1999; Masumoto et al., 2001). In contrast, the EKE
489 vertical distribution in B shows a structure that is quite typical of the mean flow profile in
490 the Labani Channel (Fig. 10), in which the maximum value is attained at the mid
491 thermocline depth, where the vertical shear of the mean flow is strongest. The EKE in B
492 is strongest at 200 m and fades away with distance from that depth (Fig. 18a).

493 Considering how the EKE is distributed in Makassar Strait and Sulawesi Sea, we
494 propose that zone B, rather than area A in Sulawesi Sea, is the EKE source for generating
495 eddies that are trapped in the lower thermocline and propagate into the Labani Channel. If
496 area B were the eddies source, southward dispersion of EKE should be well simulated by
497 the model. To detect if there is southward energy transfer from zone B, we evaluate the
498 time evolution of EKE at a depth of 225 m, a depth that has the largest averaged EKE
499 value (Fig. 18a). The EKE temporal variability along a band of latitudes within zone B
500 demonstrates a southward propagating with a phase speed of 0.2 m/s which closely
501 matches the propagation speed of an eddy (Fig. 18b). To a first approximation, it
502 therefore can be proposed that the eddy observed in the Labani Channel is not generated

503 in the Sulawesi Sea, but rather originating from just to the north of the channel in the
504 Makassar Strait at latitudes varying from 0.5°S to 2°S.

505 The next questions are why the eddy-like motions are formed at latitudes which fall
506 within range of 0.5°-2°S in the Makassar Strait lower thermocline? And how they are
507 initiated? As mentioned in the earlier discussion on eddies characteristics from
508 observation, we argue that the eddy occurring at depths beneath the mid thermocline
509 layer of Makassar Strait extracts its energy from the sheared mean flow. To support the
510 argument that the eddy generation may relate to the background flow, spatial variation of
511 the time averaged speeds in Makassar Strait at two depths in which each depth represents
512 the flow at the upper thermocline and the lower thermocline respectively, is studied.
513 Figure 19 compares the spatial distribution of the model mean flow at two levels, 100 m
514 and 200 m. The background flow magnitudes at two different depths synonymously
515 display significant variations across Makassar Strait: the maximum speed at and south of
516 the Labani Channel and a clear across-strait gradient of the mean flow particularly at
517 latitudes of 0.5°-2°S. The model mean speeds at 200 m between latitudes of 0.5°-2°S,
518 clearly reveals stronger southward magnitudes and larger across-strait gradient than that
519 at 100 m. This large across-strait gradient of the mean flow at 200 m may explain why
520 the EKE at the other lower thermocline depths is noticeably substantial.

521

522 5. Discussion and Summary

523 We have described the characteristics of the 20-40 day variability observed at the
524 two INSTANT moorings deployed in the Labani Channel of Makassar Strait 2004-2006.

525 The variability is well identified from the u' datasets recorded below the central

526 thermocline depth of 125 m, as a distinct spectral peak, which resembles a blue spectrum
527 shape over the intraseasonal timescales. Comparison between u' and v' demonstrates that
528 the across-strait component of the 20-40 day variability intraseasonal feature is more
529 energetic within the thermocline. Additionally, the 20-40 day fluctuations of u' reveal
530 downward phase propagation with a speed of 25 m/day and vertical distribution of
531 energy, in which the flow at the mid thermocline depth oscillates at shorter period than it
532 does at greater depths.

533 Apart from u' , the 20-40 day variability is also evident from the temperature
534 datasets as η' continuously show monthly periodicity. The magnitude of η' is larger than
535 the lower thermocline thickness, and η' move up and down in concert although a small
536 phase difference is observed over the lower thermocline layer. Although the 20-40 day
537 variability is not prominent in v' , it does typify the $\partial v'/\partial x$ variation over the lower
538 thermocline depths. The $\partial v'/\partial x$ time series exhibit strong correlations with u' which
539 leads us to propose that the 20-40 day variability is linked to eddy-like features. As
540 discussed previously, the velocity structure of a theoretical vortex approximates well the
541 observations and the relationship between the measured parameters. Moreover the link
542 between ζ' and η' , the isopycnals dip down (elevated) as the relative vorticity
543 magnitudes turn negative (positive) may also signify the presence and role of an eddy to
544 conserve the potential vorticity within the water column in the Labani Channel.

545 If an eddy forces the 20-40 day variability within the lower thermocline layer, why
546 does the variability at the top of the lower thermocline has strongest energy at a period of
547 25-day while the variability at the base of the lower thermocline attains maximum energy
548 at a period of 30-day? In other word, the spectral peak attributed to the 20-40 day

549 variability is centered at periods varying from 25-day at the mid thermocline depth to 30-
550 day at the base of the lower thermocline depth. Here, we suggest a Doppler effect may
551 better explain the pattern in question than the motion's natural frequencies. Referring to
552 the general dispersion relation for gravity waves, natural frequencies of motions that a
553 strait inherently can sustain is inversely proportional to the strait's width,

554 $\omega = \sqrt{(\pi g(n+1)L^{-1})\tanh((n+1)\pi HL^{-1})}$, where H , L , g , and n denote water depth, strait's
555 width, gravity and mode number, respectively. The relationship between the natural
556 frequency and the strait's width thereby indicate that as strait's width decreases with
557 depth, natural frequencies (periods) would get larger (smaller) with depth as natural
558 frequency is inversely proportional to strait's width. However, this increasing natural
559 frequency with narrower width relationship does not fit well in the Labani Channel
560 because the dominating frequency gets smaller as the channel's width decreases with
561 depth. Another physical process that may explain increasing periods of fluctuations with
562 depth is Doppler phase shift. If the 20-40 day event is advected southward with the
563 background flow, the feature is advected into the mooring sites with varying speeds over
564 depths, following the vertical structure of the mean flow (Fig. 10), which is maximum at
565 the mid thermocline depth and decays with distance from this depth. As consequence, the
566 observed dominant period of oscillation at the mid thermocline depth is shorter than that
567 at deeper levels in which the 20-40 day variability propagates at a slower pace.

568 An eddy-resolving model further supports that the 20-40 day variability observed in
569 the Labani Channel of Makassar Strait is driven by eddies. The model horizontal flow
570 and ζ' fields show that a positive (negative) ζ' event observed in the channel does
571 correspond with an anti-cyclonic (cyclonic) eddy that originates in Makassar Strait at

572 latitudes between 0.5° - 2° S, just to the north of the mooring site, a region with the largest
573 EKE. The EKE vertical distribution within this band of latitudes demonstrates strongest
574 EKE magnitude at depths greater than 200 m. The area and depths with the largest EKE
575 also coincides with the latitudes and levels at which the across-strait gradient of the
576 model background flow may provide the necessary energy for the eddy formation in
577 Makassar Strait.

578 To summarize, we suggest that a cyclonic or an anti-cyclonic eddy generated at
579 latitudes between 0.5° - 2° S in Makassar Strait explains strong signatures of the 20-40 day
580 variability in the across-strait flow and the temperature fluctuations observed within the
581 lower thermocline of the Labani Channel. The generation mechanism of the eddy is likely
582 through instability in which the required energy is supplied by the across-strait shear of
583 along-strait flow, marking the ITF. The eddy is trapped in the lower thermocline because
584 those are depths the EKE and the sheared background flow is found most energetic. The
585 eddy propagates southward along with the ITF and dissipates its energy in the Labani
586 Channel.

587

588

589

590

591

592

593

594

595 Acknowledgements

596 This work is supported by the National Science Foundation grant OCE-0219782 and
597 OCE-0725935. Bruce Huber is acknowledged for helping the preparation of gridded
598 current datasets. The HYCOM component of this article is a contribution from the "6.1
599 Dynamics of the Indonesian Throughflow (ITF) and Its Remote Impact" project
600 sponsored by the Office of Naval Research under program element number 61153N.
601 Grants of computer time were provided by the Department of Defense (DoD) High
602 Performance Computing Modernization Program and the simulations were performed on
603 the IBM Power 4+ (Kraken), the IBM Power 6 (daVinci) and the Cray XT5 (Einstein) at
604 the Navy DoD Supercomputing Resources Center, Stennis Space Center, MS. This is
605 Lamont-Doherty contribution number xxxx and NRL contribution NRL/JA/7320-11-
606 7364. This publication has been approved for public release and distribution is unlimited
607

608 References

- 609 Gordon, A.L. and Kamenkovich, V.M., 2010. Modelling and observing the Indonesian
610 Throughflow. A special issue of Dynamics of Atmosphere and Ocean. Dyn. Atmos.
611 Oceans, doi: 10.1016/j.dynatmoce.2010.04.003.
- 612 Gordon, A.L., Sprintall, J., Van Aken, H.M., Susanto D., Wijffels, S., Molcard, R.,
613 Ffield, A., Pranowo, W. and Wirasantosa, S., 2010. The Indonesian Throughflow
614 during 2004-2006 as Observed by the INSTANT program. Dyn. Atmos. Oceans,
615 doi: 10.1016/j.dynatmoce.2009.12.002.
- 616 Gordon, A.L. and Susanto, R.D., 1999. Makassar Strait Transport: Initial Estimate Based
617 on Arlindo Results. Mar. Tech. Society, 32, 34-45.
- 618 Gordon, A.L. and Fine, R. A., 1996. Pathways of Water between the Pacific and Indian
619 Oceans in the Indonesian Seas. Nature, 379, 146-149, doi: 10.1038/379146a0.
- 620 Gordon, A.L., Susanto, R.D., Ffield, A., Huber, B.A., Pranowo, W. and Wirasantosa, S.,
621 2008. Makassar Strait Throughflow, 2004 to 2006. Geophys. Res. Lett., 35,
622 L24605, doi: 10.1029/2008GL036372.

623 Lilly, J.M. and Rhines, P.B., 2002. Coherent Eddies in the Labrador Sea Observed from a
624 Mooring. *J. Phys. Oceanogr.*, 32, 585-598, doi: 10.1175/1520
625 0485(2002)032<0585:CEITLS>2.0.CO;2.

626 Masumoto, Y., Kagimoto, T., Yoshida, M., Fukuda, M., Hirose, N. and Yamagata, T.,
627 2001. Intraseasonal eddies in the Sulawesi Sea simulated in an ocean general
628 circulation model. *Geophys. Res. Lett.*, 28(8), 1631-1634.

629 Metzger, E.J., Hurlburt, H.E., Xu, X., Shriver, J.F., Gordon, A.L., Sprintall, J., Susanto,
630 R.D. and Van Aken, H.M., 2010. Simulated and Observed Circulation in the
631 Indonesian Seas: 1/12° Global HYCOM and the INSTANT Observations. *Dyn.*
632 *Atmos. Oceans*, 57, 275-300, doi: 10.1016/j.dynatmoce.2010.04.002.

633 Pujiana, K., Gordon, A.L., Sprintall, J. and Susanto, R.D., 2009. Intraseasonal variability
634 in the Makassar Strait Thermocline. *J. Mar. Res.*, 67, 757-777.

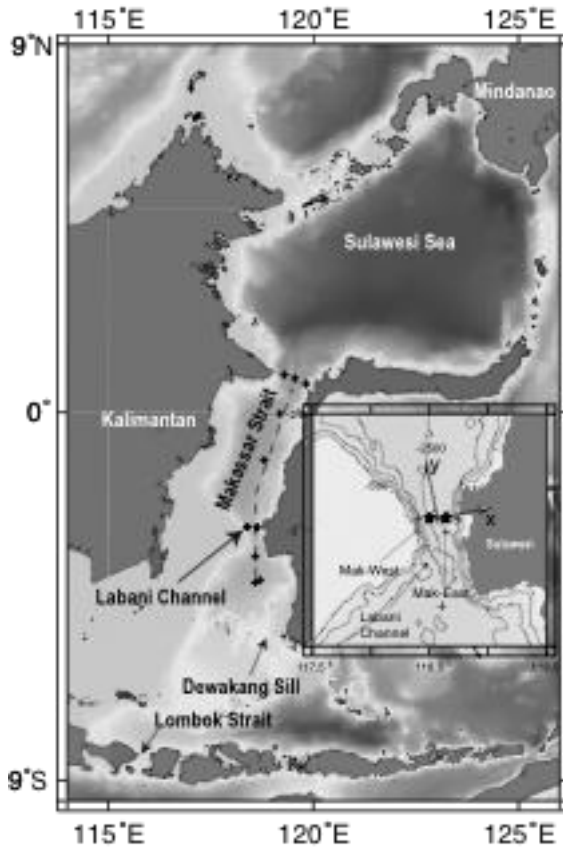
635 Qiu, B., Mao, M. and Kashino, Y., 1999. Intraseasonal Variability in the Indo-Pacific
636 Throughflow and the Regions Surrounding the Indonesian Seas. *J. Phys. Oceanogr.*,
637 29, 1599-1618, doi: 10.1175/1520-0485(1999)029<1599:IVITIP>2.0.CO;2.

638 Susanto, R.D., Gordon, A.L., Sprintall, J. and Herunadi, B., 2000. Intraseasonal
639 Variability and Tides in Makassar Strait. *Geophys. Res. Lett.*, 27(10), 1499-1502,
640 doi: 10.1029/2000GL011414.

641 Sprintall, J., Wijffels, S., Gordon, A.L., Ffield, A., Molcard, R., Susanto, R.D., Soesilo,
642 I., Sopaheluwakan, J., Surachman, Y. and Van Aken, H., 2004. INSTANT: A New
643 International Array to Measure the Indonesian Throughflow. *Eos Trans.*
644 *AGU*, 85(39), doi: 10.1029/2004EO390002.

645

646 Figures



647

648

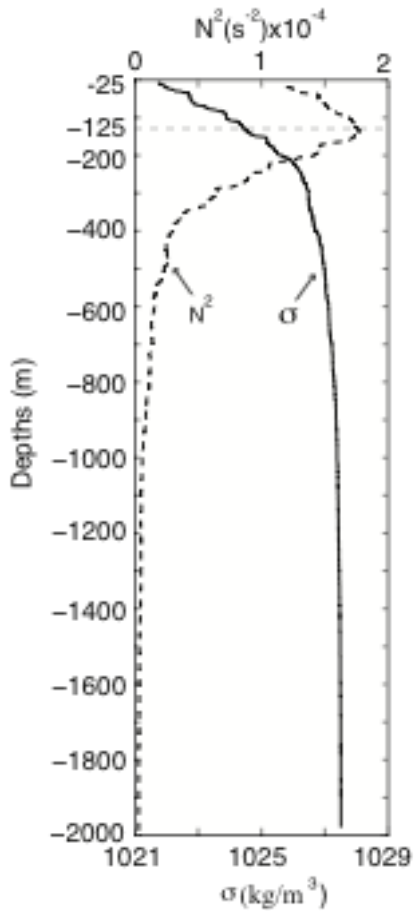
649 Figure 1. Locations of point measurements in Makassar Strait. The moorings are shown
650 as stars and are deployed in the Labani Channel, a constriction in Makassar Strait.

651 Crosses denote CTD casts during 1996-1998. Inset displays an expanded view of the
652 Labani Channel, the major and minor axes of the channel, and the mooring sites (Mak-
653 West and Mak-East). The along-strait axis (y) and across-strait axis (x) is tilted 10°
654 counterclockwise relative to the geographic north and east respectively.

655

656

657



658

659 Figure 2. The average vertical structure of the interior Makassar Strait inferred from
 660 several CTD casts during 1993-1998 given in Figure 1. The average of potential density
 661 (σ , solid line) and buoyancy frequency (N^2 , dashed line). The buoyancy frequency is
 662 computed using, $N^2 = -(g/\rho_o)\partial\sigma/\partial z$, where g is gravitational acceleration and ρ_o is
 663 vertically averaged potential density.

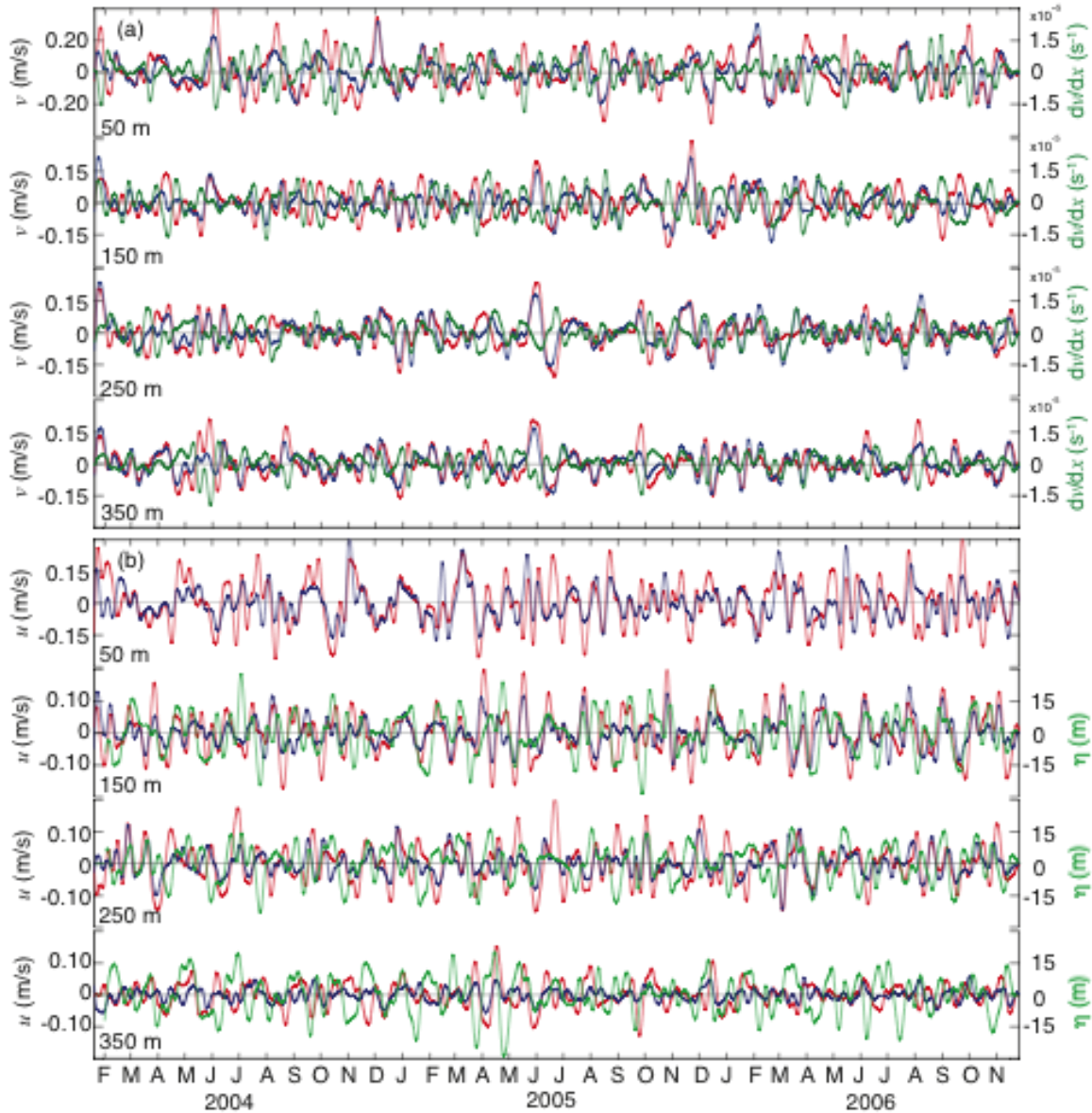
664

665

666

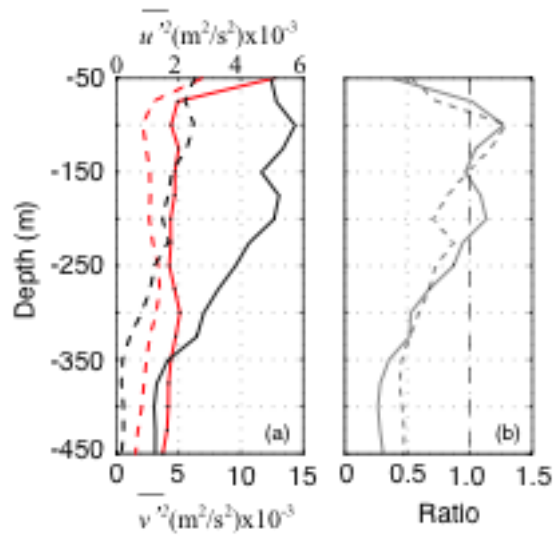
667

668



669

670 Figure 3. Time series of u , v , dv/dx , and η varying at intraseasonal timescales for selected
 671 depths from Mak-West and Mak-East moorings. A bandpass filter with cut off periods of
 672 20 and 90 days is applied to isolate intraseasonal signals from the raw data. (a) displays v
 673 at Mak-West (red) and Mak-East (blue) and dv/dx (green) variability, where dv is the
 674 difference between $v_{\text{Mak-East}}$ and $v_{\text{Mak-West}}$ and dx is the distance between the moorings. The
 675 distance of the two moorings is ~ 19 km. (b) demonstrates u at Mak-west (red) and Mak-
 676 east (blue) and η (green).



677

678 Figure 4. (a) Profiles of variances attributed to u' and v' at intraseasonal timescales (20-
 679 90 days) within the Mak-West and Mak-East thermocline. Solid and dashed black (red)
 680 lines show the variances of u' (v') observed at Mak-West and Mak-East moorings
 681 respectively. (b) Ratio of u' and v' variances given in (a). Solid line is for the ratio of u'
 682 and v' at Mak-West mooring, and dashed line is for the ratio of u' and v' at Mak-East
 683 site.

684

685

686

687

688

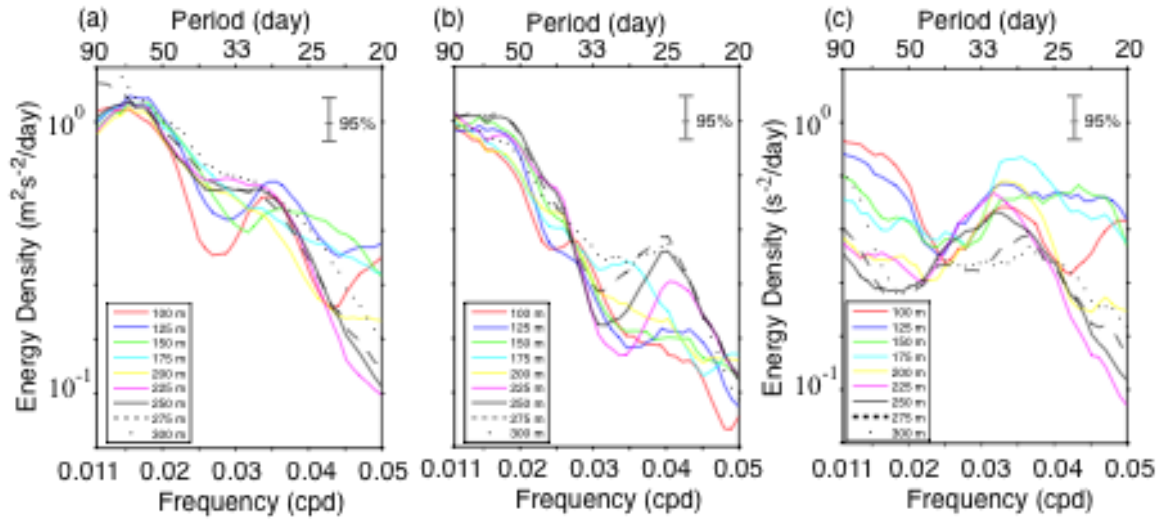
689

690

691

692

693



694

695 Figure 5. Multitaper spectral estimates of v' observed at different levels in the Mak-West
 696 (a) and Mak-East (b) lower thermocline during 2004-2006. (c) displays spectral estimates
 697 of across-strait gradient of v' , computed by subtracting v' observed at Mak-East from
 698 that observed at Mak-West. Error bars on the spectral estimates mark the 95% confidence
 699 limits.

700

701

702

703

704

705

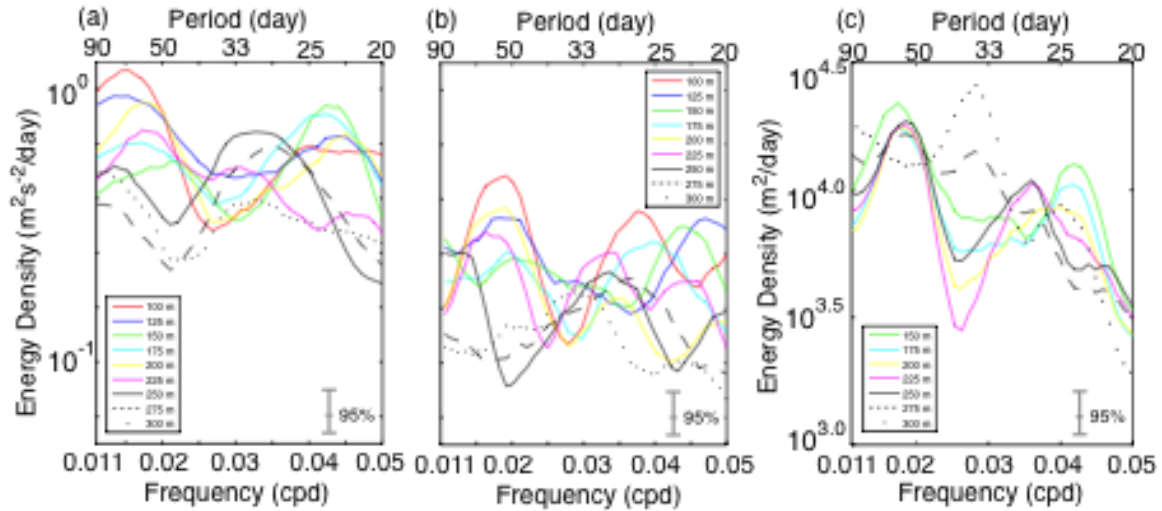
706

707

708

709

710



711

712 Figure 6. Multitaper spectral estimate of u' and η at several levels from Mak-West and
 713 Mak-East moorings within the lower thermocline of Makassar Strait during 2004-2006.

714 (a) and (b) illustrate spectral estimate of u' for Mak-West and Mak-East respectively. (c)

715 displays spectral estimates of η for Mak-West. Error bars on the spectral estimates mark
 716 the 95% confidence limits.

717

718

719

720

721

722

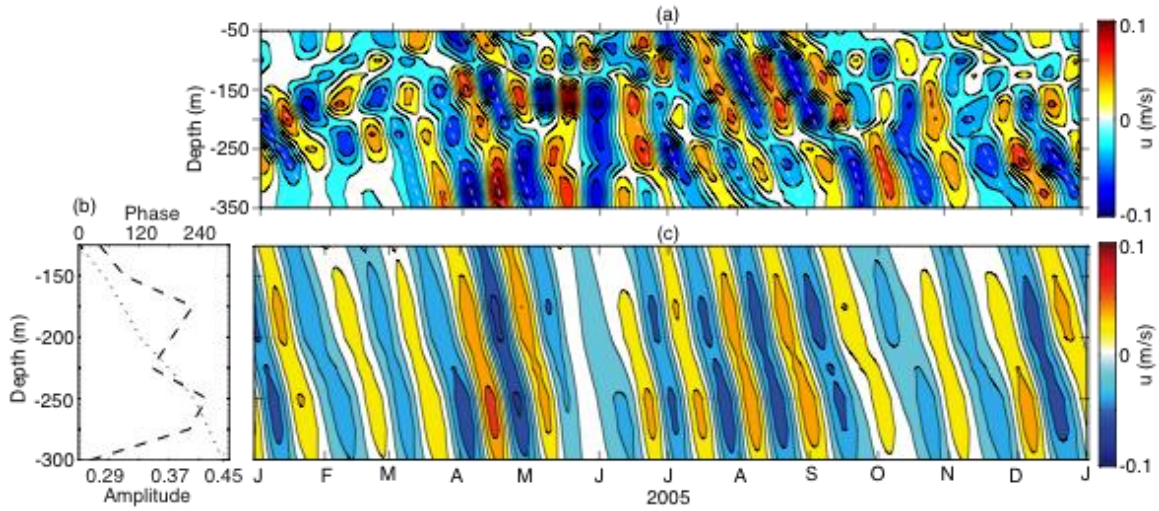
723

724

725

726

727



728

729 Figure 7. Across-strait flow varying at periods of 20-40 days observed at Mak-West

730 mooring in 2005 (a) and its orthogonal function approximation (b, c). Dashed lines in (a)

731 show phase lines. Dashed and dotted lines in (b) show the 1st eigenvector and its relative

732 phase that represents 50% variance of (a). (c): Reconstructed across-strait flow for the 1st

733 mode.

734

735

736

737

738

739

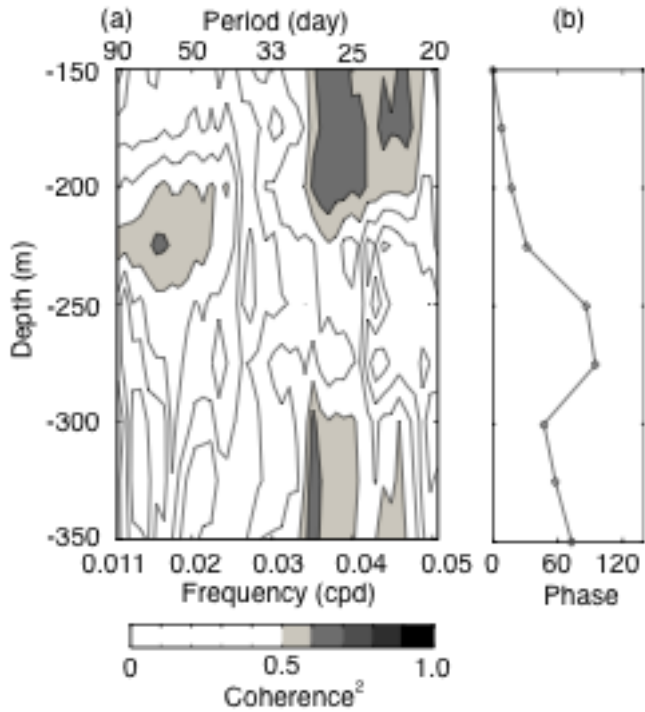
740

741

742

743

744



745

746 Figure 8. The degree of coherence between u' and η at intraseasonal timescales over the
 747 lower thermocline of Mak-West. Amplitudes of coherence squared (a) are shaded for
 748 values larger than 95% significance level, while phase relatives (b) are averaged over a
 749 period band of 20-40 days.

750

751

752

753

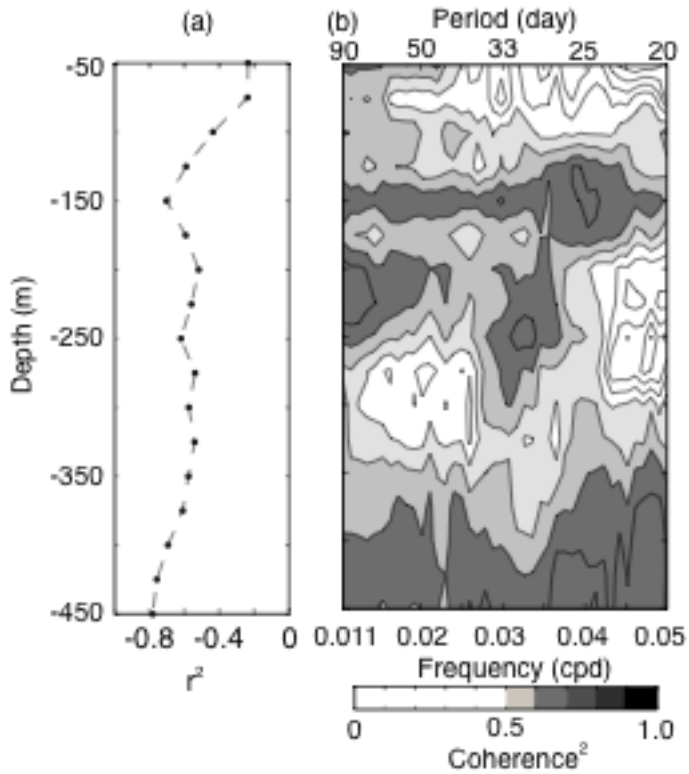
754

755

756

757

758



759

760 Figure 9. The degree of correlation between v' and u' at intraseasonal timescales over the
 761 Mak-West thermocline. (a): Zero-lag coefficients obtained from time-lagged cross
 762 correlation analysis. (b): Amplitudes of coherence squared are shaded for values larger
 763 than 95% significance level.

764

765

766

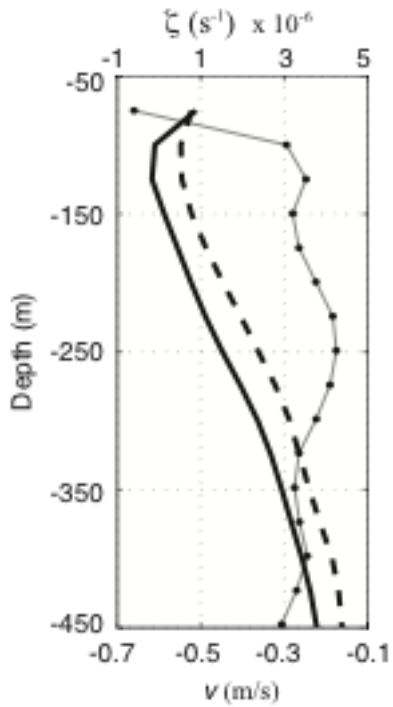
767

768

769

770

771



772

773 Figure 10. Vertical structure of the background flow observed at Mak-West (solid line)
 774 and Mak-East (dashed line) and its corresponding relative vorticity (dotted line). The
 775 background flow at a certain depth is the time average of subinertial flow, which is
 776 obtained through applying a butterworth low-pass filter to the velocity field dataset with a
 777 cut-off period of 9.5-day (inertial period at the mooring site).

778

779

780

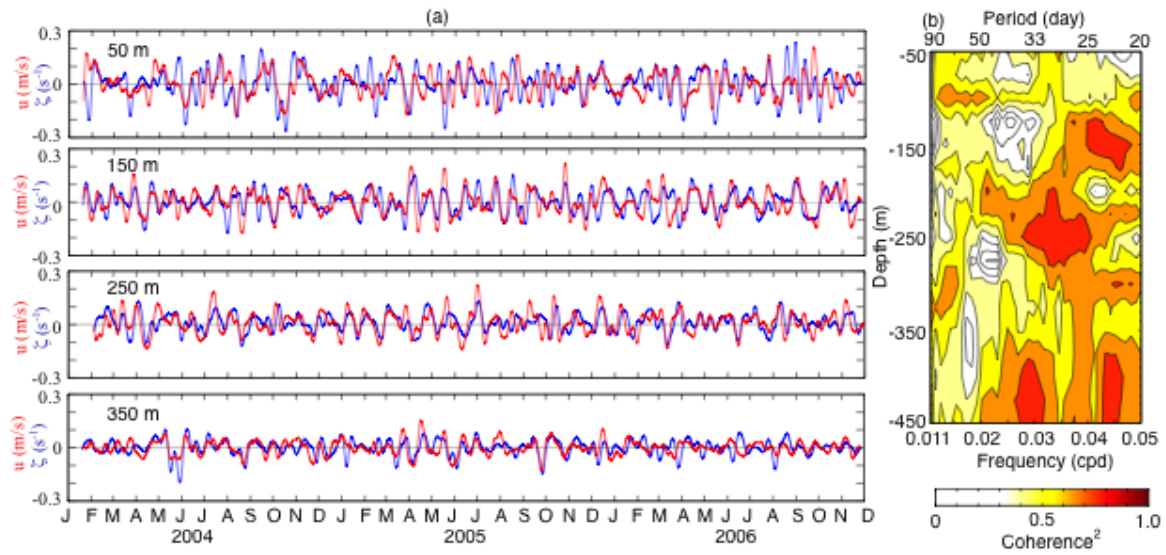
781

782

783

784

785



786

787 Figure 11. (a) Plots of ζ' and u' varying at intraseasonal timescales for several depths.

788 ζ' is defined as across-strait gradient of v' observed at Mak-West and Mak-East sites,

789 while u' is from Mak-West mooring. (b): Amplitudes of coherence squared between ζ'

790 and u' across intraseasonal periods and over thermocline depths, and they are given in

791 color for values that exceed 95% significance level.

792

793

794

795

796

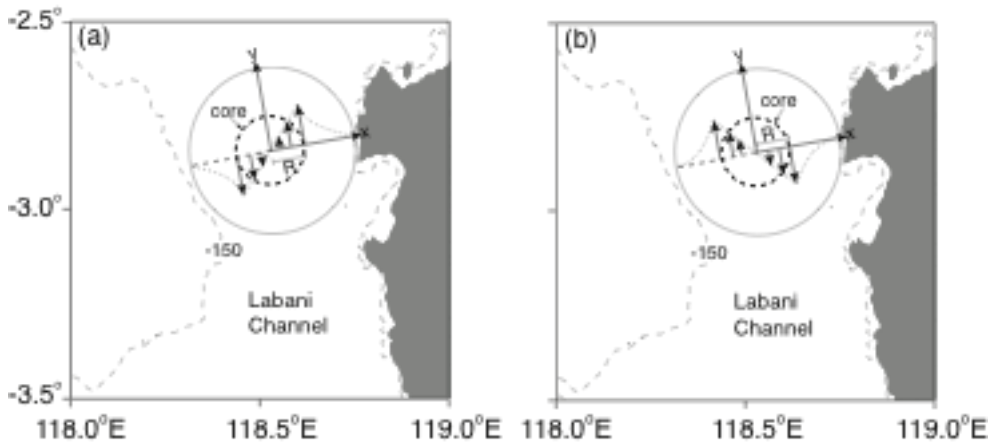
797

798

799

800

801



802

803 Figure 12. Schematic of anti-cyclonic (a) and cyclonic eddy (b) propagating in the Labani

804 Channel. The eddy has a core of radius R (dashed circle). Dotted lines show the velocity

805 structure of an ideal Rankine vortex.

806

807

808

809

810

811

812

813

814

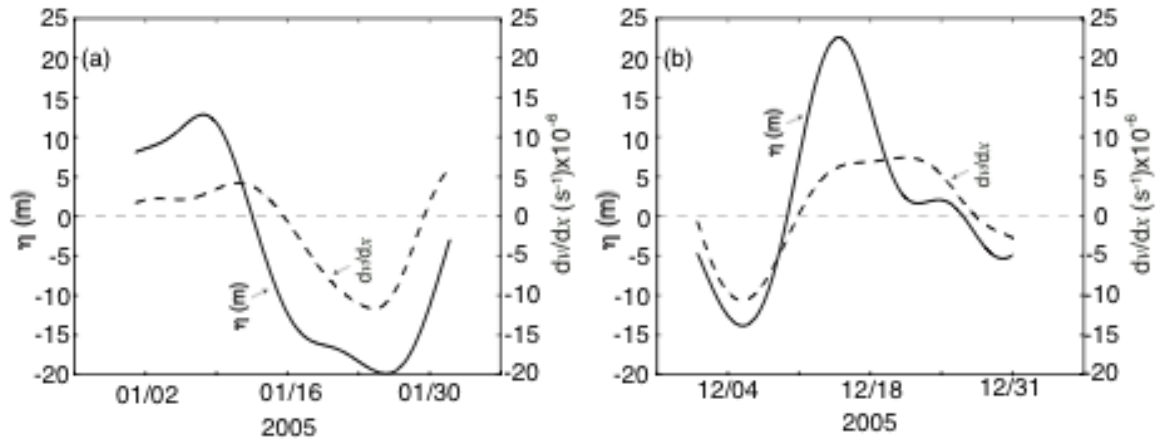
815

816

817

818

819



820

821 Figure 13. Temporal variability of relative vorticity (dv/dx) and isotherm vertical
 822 displacement (η) at depth of 150 m observed from the moorings in the Labani Channel.

823 (a) demonstrates how a motion with negative dv/dx corresponds with a minimum η on 24
 824 January 2005, while (b) illustrates the relationship between a positive dv/dx motion and a
 825 maximum η on 17 December 2005.

826

827

828

829

830

831

832

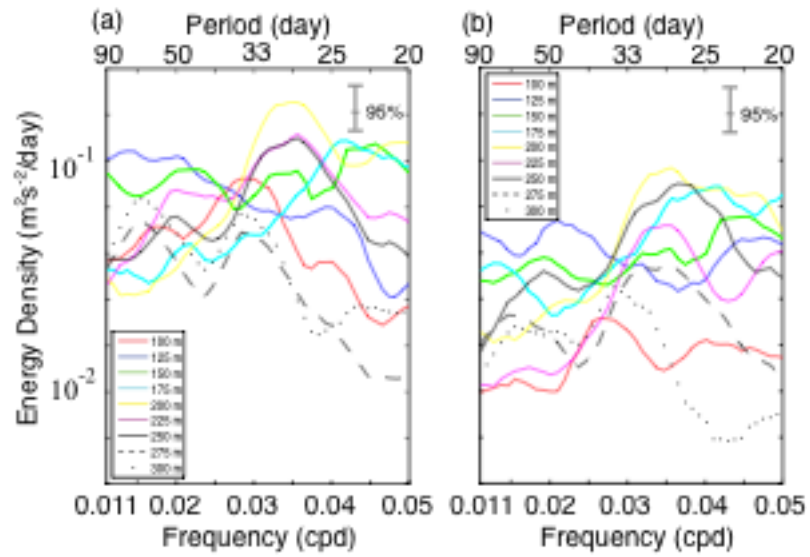
833

834

835

836

837



838

839 Figure 14. Multitaper spectral estimates of simulated u' at intraseasonal timescales for
 840 several depths at the Mak-West (a) and Mak-East (b) locations in Makassar Strait. Error
 841 bars on the spectral estimates mark the 95% confidence level.

842

843

844

845

846

847

848

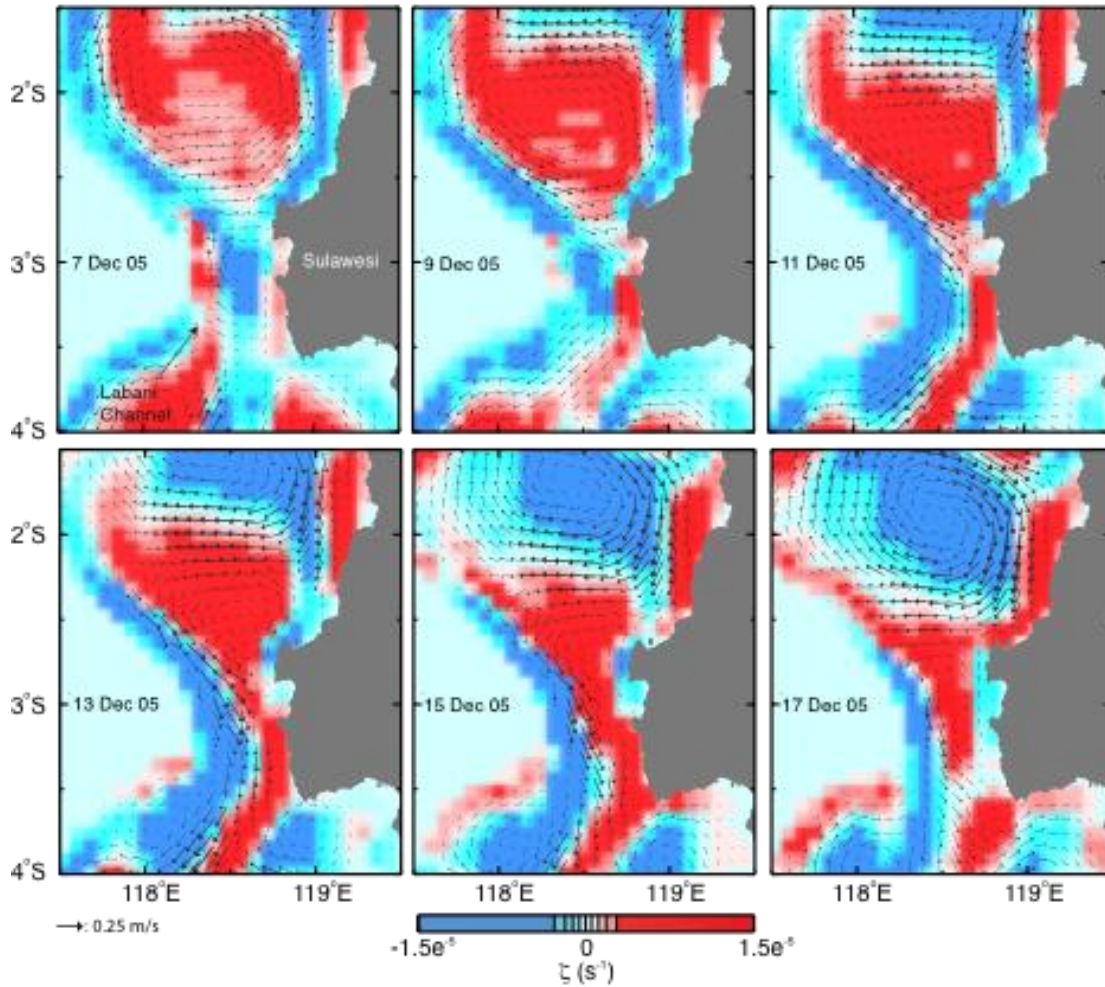
849

850

851

852

853



854

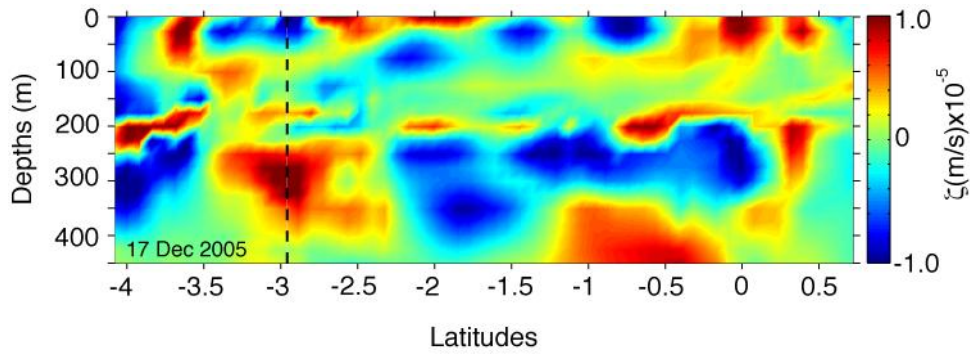
855 Figure 15. Snapshots of the model horizontal flow field (arrow) and its corresponding
 856 vorticity field (in color) at 250 m in the vicinity of the Labani Channel for several days in
 857 December 2005. The current vectors are for periods of 20-40 days. The stars denote the
 858 mooring sites.

859

860

861

862



863

864 Figure 16. The model ζ' plot for several depths along a transect in Makassar Strait
 865 shown in Figure 1, simulated on 17 December 2005. The ζ' time series are computed
 866 using horizontal velocities for intraseasonal timescales. The dashed line indicates the
 867 latitude of the mooring location in the Labani Channel.

868

869

870

871

872

873

874

875

876

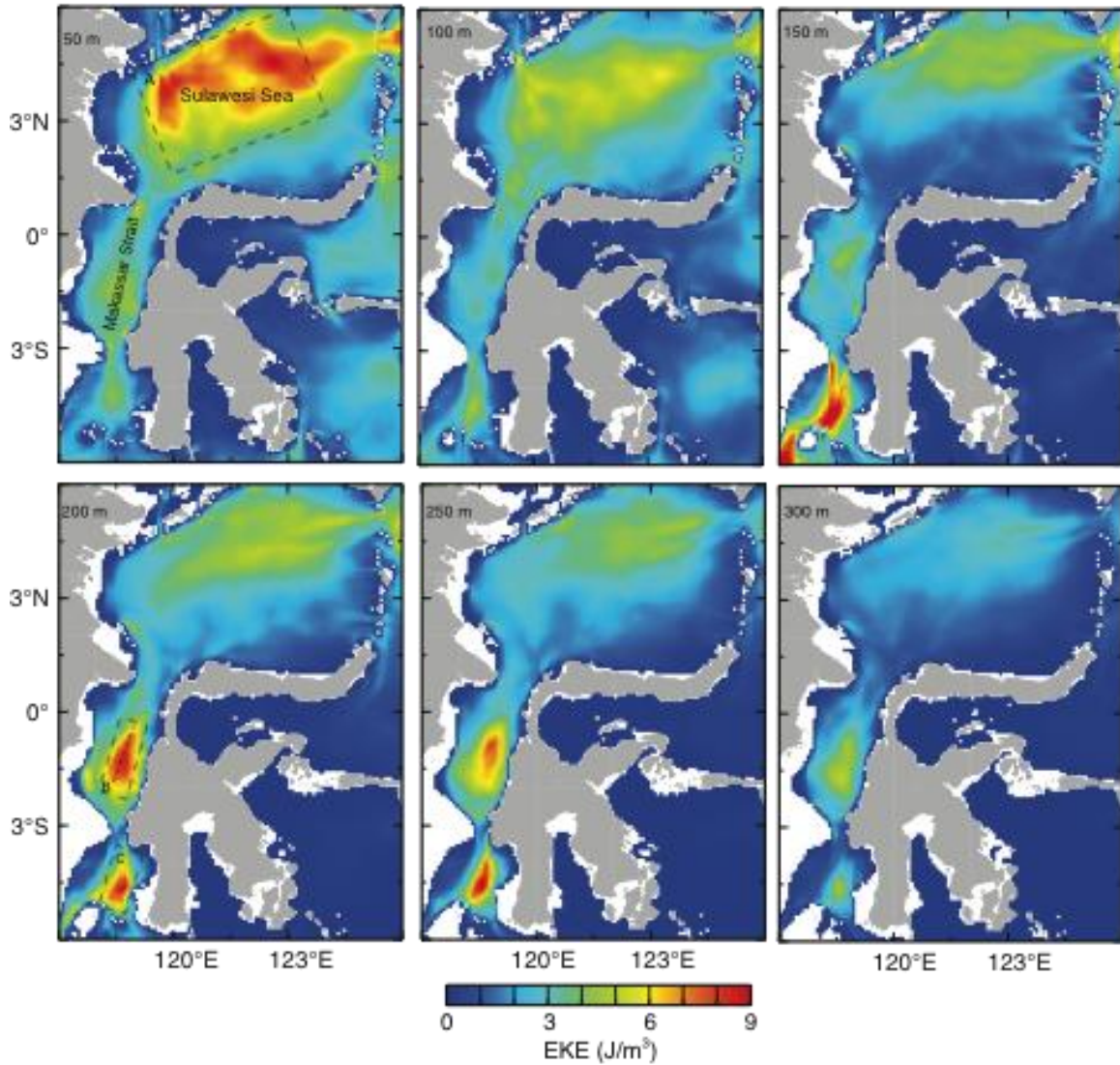
877

878

879

880

881



882

883 Figure 17. Plots of the averaged EKE simulated at several depths within the Makassar

884 Strait and Sulawesi Sea thermocline. The mean EKE is computed for a 3-year period

885 from 2004 to 2006. Dashed box represents a region with the most energetic EKE.

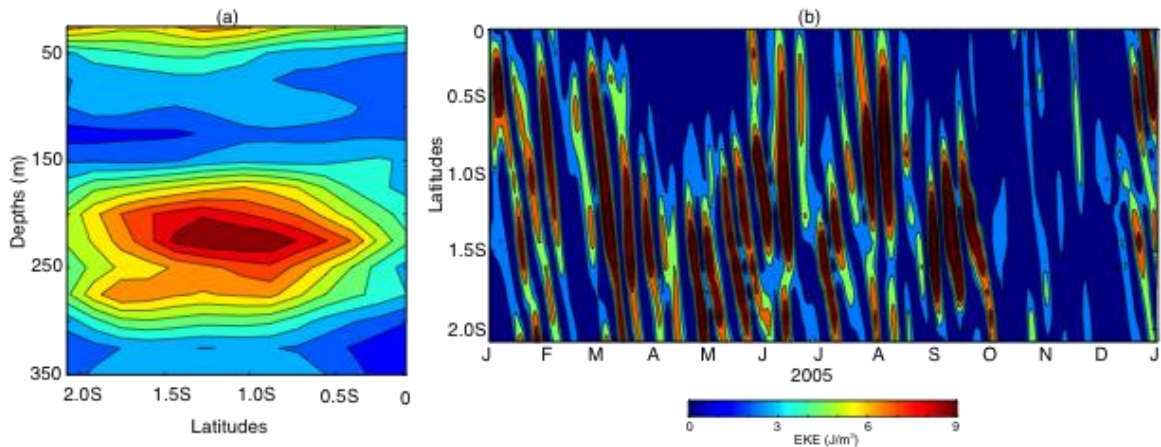
886

887

888

889

890



891

892 Figure 18. (a) A vertical distribution plot of the mean EKE simulated at several latitudes
 893 within zone B given in Figure 17. (b) The temporal variability of the model EKE at depth
 894 of 250 m for several latitudes along a transect within zone B shown in Figure 17.

895

896

897

898

899

900

901

902

903

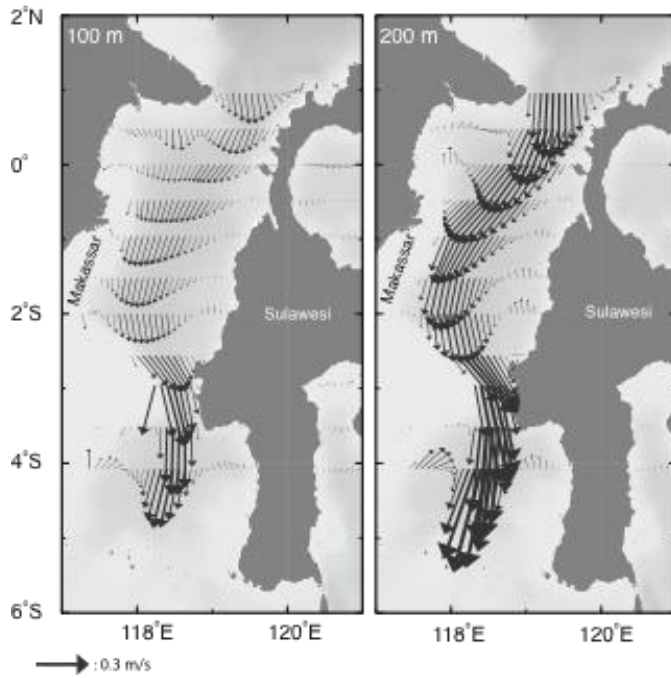
904

905

906

907

908



909

910 Figure 19. The model background flow at two different depths simulated in Makassar
 911 Strait. The mean flow is obtained through applying a butterworth low-pass filter to the
 912 model raw data with a cutoff period of 90-day.